Commun. Comput. Phys.
doi: 10.4208/cicp.OA-2016-0189

Vol. **23**, No. 3, pp. 747-772
March 2018

An Energy Conserving Local Discontinuous Galerkin Method for a Nonlinear Variational Wave Equation

Nianyu Yi[1] and Hailiang Liu[2,*]

[1] *School of Mathematics and Computational Science, Xiangtan University, Xiangtan 411105, P.R. China.*
[2] *Department of Mathematics, Iowa State University, Ames, IA 50011, USA.*

Received 1 November 2016; Accepted (in revised version) 30 May 2017

Abstract. We design and numerically validate a local discontinuous Galerkin (LDG) method to compute solutions to the initial value problem for a nonlinear variational wave equation originally proposed to model liquid crystals. For the semi-discrete LDG formulation with a class of alternating numerical fluxes, the energy conserving property is verified. A dissipative scheme is also introduced by locally imposing some numerical "damping" in the scheme so to suppress some numerical oscillations near solution singularities. Extensive numerical experiments are presented to validate and illustrate the effectiveness of the numerical methods. Optimal convergence in L^2 is numerically obtained when using alternating numerical fluxes. When using the central numerical flux, only sub-optimal convergence is observed for polynomials of odd degree. Numerical simulations with long time integration indicate that the energy conserving property is crucial for accurately capturing the underlying wave shapes.

AMS subject classifications: 65M60, 65M12, 35Q35

Key words: Discontinuous Galerkin method, variational wave equation, energy conservation.

1 Introduction

Many applications involve the solution of wave equations. In this paper, we consider a variational nonlinear wave equation that models the propagation of orientation waves in the director field in nematic liquid crystals. Let the director filed $n(x,t)$ be the orientation of the molecules at each location x and time t, in planar deformations of nematic liquid crystals involving only one-dimensional space variable, the director field is given by

$$n(x,t)=\cos u(x,t)e_x+\sin u(x,t)e_y,$$

*Corresponding author. *Email addresses:* yinianyu@xtu.edu.cn (N. Yi), hliu@iastate.edu (H. Liu)

where e_x and e_y are the coordinator vectors in the x and y directions, respectively. In such a setting, the dynamics of the liquid crystal is described by some unknown function $u(x,t)$, which represents the angle of the director field relative to the x-direction, and the variational principle [28] reduces to the following nonlinear wave equation

$$\partial_t^2 u - c(u)\partial_x(c(u)\partial_x u) = 0, \tag{1.1}$$

and the wave speed $c(u)$ is given by

$$c^2(u) = \alpha\cos^2 u + \beta\sin^2 u$$

for some positive constant α,β. In general, we assume that $c(u)$ is a smooth, uniformly positive function. One of the most important properties of the wave equation is the conservation of energy. Indeed, the analysis in [5,6,24] shows that conservative solutions are unique, globally defined, and yield a flow on the space of couples $(u,u_t)\in H^1(\mathbb{R})\times L^2(\mathbb{R})$. For each conservative solution, the total energy

$$E(t) = \frac{1}{2}\int (\partial_t u(x,t)^2 + (c(u(x,t))\partial_x u(x,t))^2)dx$$

remains constant in time. Aim of this work is to compute such a conservative solution to (1.1) with an arbitrary high order of accuracy.

Note that smooth solutions may well develop singularities in finite time [17]. It was observed in [6, 24] that conservative solutions can occasionally be measure-valued. On the other hand, for dissipative solutions, studied in [7, 17, 33, 34], the continuous dependence for general initial data in $H^1\times L^2$ remains an open question. Nevertheless, when singularity occurs in solutions, the numerical approximation to u_x may become oscillatory. We therefore also propose a dissipative scheme by locally imposing some numerical "damping" in the conservative scheme, in such a way that it not only indicates where the singularity is located, but it also provides a measure for the artificial damping that smoothens singularities. Relatively little dissipation is added in the smooth regions away from the singularity to ensure an accurate computation of solution structures away from singularities.

Existing numerical results for wave propagation reveal that energy conserving numerical methods, which conserve the discrete approximation of energy, are favorable because they are able to maintain the phase and shape of the waves accurately. Numerical methods without this property may result in substantial phase and shape errors after long time integration.

A vast amount of literature can be found on the numerical approximation of wave equations, including finite difference, finite element, finite volume, spectral methods and integral equation based methods. In this paper, we will confine our attention to the discontinuous Galerkin (DG) method, which is a class of finite element methods using completely discontinuous piecewise-polynomial space for the numerical solution and the test functions in the spatial variables. Various DG methods have been designed for first order

hyperbolic systems, mostly with entropy satisfying numerical fluxes so that the scheme is entropy stable [11–14]. Chung and Engquist [8, 9] have proposed an optimal, energy conserving DG method for the first-order wave equation using staggered grids. They introduced different meshes for different computational variables, and are able to prove the optimal convergence for unstructured meshes.

DG methods for solving the second-order linear wave equation have been proposed in a variety of forms: a family of non-symmetric interior penalty (IP) DG method was developed in [27], in which the dissipative mechanism in the method depends on the choice of an interior penalty parameter. The symmetric IPDG method is proposed for the numerical discretization of the second-order wave equation in [19]. Recently, an energy conserving local discontinuous Galerkin scheme was proposed first in [29] for the linear wave equation with constant speed, further extension to the linear wave equation $u_{tt}=(c^2(x)u_x)_x$, but with piecewise smooth speed function $c(x)$ is presented in [10] — in both papers the split system $u_{tt}=(c(x)w)_x, w=c(x)u_x$ is used. A different DG formulation based on $w=u_t, w_t-c^2(x)u_{xx}=0$ with a special testing on the equation $w-u_t=0$ was recently proposed in [1] to conserve or dissipate the energy for a large class of systems of linear equations of second order.

For the nonlinear second order wave equation (1.1), a semi-discrete finite difference scheme was first considered in [22], where the authors were able to prove convergence of the generated numerical solution to the dissipative solution, for some restricted choice of $c(u)$. Further in [25] finite difference schemes for approximating the variational wave equation in both one and two space dimensions were developed. The obtained energy conservative (dissipative) schemes are based on rewriting the wave equation as a first-order system of equations in terms of $u_t \pm c(u)u_x$, which have already been explored in analysis, see, e.g., [6, 24]. Still based on the first order hyperbolic system, the authors in [3] proposed both energy conserving and dissipative DG methods, with the dissipation provided by a smoothness indicator and a numerical flux. Numerical experiments using a Fourier pseudospectral method are conducted in [20] to compute both conservative and dissipative solutions, with energy-conserving discretization as well as with a vanishing viscosity sequence.

In this paper, we consider a generalized wave equation imposed on a bounded domain subject to proper boundary conditions. Usually it is difficult to obtain DG schemes for second order wave equations which conserve energy to be optimally high order accurate. Here, we apply the LDG discretization to the system of $u_{tt}=c(u)q_x, q=c(u)u_x$ for this nonlinear wave problem, similar to the reformulation in [29] for the linear wave equation. The proposed semi-discrete scheme is shown to be energy conserving. Coupled with the centered second-order time discretization (the leap-frog method) for the temporal derivatives, we present the fully discrete LDG method. In our dissipative DG scheme, the dissipation is provided by only a smoothness indicator.

The rest of this paper is organized as follows: In Section 2 we present the energy conserving LDG method, and a dissipative scheme is discussed in Section 3. Section 4 is devoted to numerical experiments with various examples. To demonstrate the importance

of energy conservation, we test an example with long time integration, and the numerical results reveal that our method stays very accurate after long time integration, in contrast to numerical methods without this property. The advantage of energy-conserving methods is to solve wave problems, with the attempt to resolve all wave patterns for long time periods.

2 The local discontinuous Galerkin method

2.1 Reformulation

We consider a generalized nonlinear wave equation of the form

$$\partial_t^2 u - c(u)\partial_x(c(u)\partial_x u) + V'(u) = 0, \tag{2.1}$$

where $V(u)$ is a given function, subject to the initial data

$$u(x,0) = u_0(x), \quad \partial_t u(x,0) = u_1(x), \quad x \in I, \tag{2.2}$$

and periodic boundary conditions. Here I is a bounded interval in $\mathbb{R}$. Note that this system can be identified as the Euler-Lagrangian equation derived from the action principle associated with the Lagrangian $\frac{1}{2}|\partial_t u|^2 - \frac{1}{2}c^2(u)|\partial_x u|^2 - V(u)$, see, e.g. [32].

The LDG discretization will be based on the following system

$$\partial_t^2 u = c(u)\partial_x q - V'(u), \tag{2.3a}$$
$$q = c(u)\partial_x u, \tag{2.3b}$$

for which the energy of the wave equation becomes

$$E = \int_I \left(\frac{1}{2}((\partial_t u)^2 + q^2) + V(u) \right) dx. \tag{2.4}$$

2.2 Semi-discrete LDG formulation

We develop an energy conserving local discontinuous Galerkin (ECLDG) method for (2.1), (2.2) through the reformulation (2.3). Let us denote the computational mesh by $I_j = (x_{j-1/2}, x_{j+1/2})$ for $j = 1, \cdots, N$. The center of the cell is $x_j = (x_{j-1/2} + x_{j+1/2})/2$, and $h_j = x_{j+1/2} - x_{j-1/2}$. We denote by $w^+_{j+1/2}$ the value of w at $x_{j+1/2}$ evaluated from the right element I_{j+1}, and $w^-_{j+1/2}$ the value of w at $x_{j+1/2}$ evaluated from the left element I_j. $[w] = w^+ - w^-$ denotes the jump of w at cell interfaces, and $\{w\} = \frac{1}{2}(w^+ + w^-)$ denotes the average of the left and right interface values. We then define the piecewise polynomial space V_h as the space of polynomials of degree k in each cell I_j, i.e.,

$$V_h = \left\{ w : w \in P^k(I_j) \text{ for } x \in I_j, j = 1, \cdots, N \right\}.$$

Denote $C(u)=\int^u c(s)ds$, the nonlinear system (2.3) becomes

$$\partial_t^2 u = c(u)\partial_x q - V'(u), \tag{2.5a}$$
$$q = \partial_x(C(u)). \tag{2.5b}$$

Integration of (2.5) against $\xi,\eta\in H^1(I)$ over I_j with integration by parts leads to

$$\int_{I_j}\partial_t^2 u\xi dx = -\int_{I_j} q\partial_x(c(u)\xi)dx + qc(u)\xi|_{\partial I_j} - \int_{I_j} V'(u)\xi dx, \tag{2.6a}$$
$$\int_{I_j} q\eta dx = -\int_{I_j} C(u)\partial_x\eta dx + C(u)\eta|_{\partial I_j}, \tag{2.6b}$$

where

$$v|_{\partial I_j} = v(x_{j+1/2}^-) - v(x_{j-1/2}^+).$$

Next we replace ξ,η by test functions in V_h and the exact solutions u,q by the numerical approximation solutions u_h,q_h. The boundary values q and $C(u)$ are replaced by the numerical fluxes $\hat{q}_h$ and $\hat{C}_h$ which will be defined latter. Thus the approximate solution is defined as

$$\int_{I_j}\partial_t^2 u_h\xi dx = -\int_{I_j} q_h\partial_x(c(u_h)\xi)dx + \hat{q}_h c(u_h)\xi|_{\partial I_j} - \int_{I_j} V'(u_h)\xi dx, \tag{2.7a}$$
$$\int_{I_j} q_h\eta dx = -\int_{I_j} C(u_h)\partial_x\eta dx + \hat{C}_h\eta|_{\partial I_j}. \tag{2.7b}$$

To derive an energy conserving scheme, we apply the integration by parts to the term $-\int_{I_j} C(u_h)\partial_x\eta dx$ once again, which leads to a scheme

$$\int_{I_j}\partial_t^2 u_h\xi dx = -\int_{I_j} q_h\partial_x(c(u_h)\xi)dx + \hat{q}_h c(u_h)\xi|_{\partial I_j} - \int_{I_j} V'(u_h)\xi dx, \tag{2.8a}$$
$$\int_{I_j} q_h\eta dx = \int_{I_j}\partial_x(C(u_h))\eta dx + (\hat{C}_h - C(u_h))\eta|_{\partial I_j}. \tag{2.8b}$$

We are now ready to state the semi-discrete conservative discontinuous Galerkin method as follows: find $u_h,q_h\in V_h$, such that $\forall\xi,\eta\in V_h$,

$$\int_{I_j}\partial_t^2 u_h\xi dx = -\int_{I_j} q_h\partial_x(c(u_h)\xi)dx + \hat{q}_h c(u_h)\xi|_{\partial I_j} - \int_{I_j} V'(u_h)\xi dx, \tag{2.9a}$$
$$\int_{I_j} q_h\eta dx = \int_{I_j} c(u_h)\partial_x u_h\eta dx + (\hat{C}_h - C(u_h))\eta|_{\partial I_j}, \tag{2.9b}$$

where the numerical fluxes are defined as

$$(\hat{q}_h,\hat{C}_h) = (q_h^\theta, C_h^{1-\theta}) := (\theta q_h^+ + (1-\theta)q_h^-, (1-\theta)C(u_h^+) + \theta C(u_h^-)), \quad \theta\in[0,1]. \tag{2.10}$$

We prepare the initial data for the ODE system (2.9) by a projection of (u_0,u_1) in each computational cell so that

$$u_h(x,0)=\Pi u_0, \qquad \partial_t u_h(x,0)=\Pi u_1. \tag{2.11}$$

Possible choices for Πv include the piecewise L^2-projection of v into V_h or the Lagrange interpolant of v in V_h. Note that the choice of the numerical flux $\hat{C}_h$ in (2.10) ensures that the term $\hat{C}_h-C(u_h)$ on cell boundaries is uniquely determined. The global form of the DG formulation may be obtained by summing (2.9) over all j's,

$$\int \partial_t^2 u_h \xi dx = -\int q_h \partial_x (c(u_h)\xi)dx - \sum_j (\hat{q}_h[c(u_h)\xi])_{j+1/2} - \int V'(u_h)\xi dx, \tag{2.12a}$$

$$\int q_h \eta dx = \int c(u_h)\partial_x u_h \eta dx + \sum_j \left([C(u_h)\eta]_{j+1/2} - (\hat{C}_h[\eta])_{j+1/2}\right), \tag{2.12b}$$

where $\int = \sum_{j=1}^N \int_{I_j}$, and the periodic boundary conditions have been used.

2.3 Energy conserving property

We now show that for any $\theta \in [0,1]$, the numerical flux (2.10) is admissible for the LDG scheme (2.9) to conserve the discrete energy (2.4).

Theorem 2.1. *For the semi-discrete approximations (u_h,q_h) obtained from the LDG formulation* (2.9) *with* (2.10)*. The semi-discrete energy*

$$E_h(t)=\int_I \left(\frac{1}{2}((\partial_t u_h)^2+q_h^2)+V(u_h)\right)dx$$

is preserved in the sense that

$$E_h(t)=E_h(0), \quad \forall t>0.$$

Proof. Let us use the notation $C_h=C(u_h)$ below. To show the conservation of E, we take $\xi=\partial_t u_h$ in (2.12a), and $\eta=q_h$ in ∂_t(2.12b) to obtain

$$\int \partial_t^2 u_h \partial_t u_h dx = -\int q_h \partial_x(\partial_t C_h)dx - \sum_j (\hat{q}_h[\partial_t C_h])_{j+1/2} - \int V'(u_h)\partial_t u_h dx,$$

$$\int \partial_t q_h q_h dx = \int \partial_x(\partial_t C_h)q_h dx + \sum_j \left([\partial_t C_h q_h]_{j+1/2} - (\partial_t \hat{C}_h[q_h])_{j+1/2}\right).$$

Adding the above together and integrating the complete derivative out, we obtain

$$\frac{d}{dt}\int \left(\frac{1}{2}(\partial_t u_h^2+q_h^2)+V(u_h)\right)dx = \sum_{j=1}^N \left([\partial_t C_h q_h]_{j+1/2} - (\partial_t \hat{C}_h[q_h])_{j+1/2} - (\hat{q}_h[\partial_t C_h])_{j+1/2}\right),$$

which vanishes, by the identity

$$[ab]=(\theta a^+ +(1-\theta)a^-)[b]+(\theta b^- +(1-\theta)b^+)[a],\quad \forall\theta\in[0,1].$$

This proof is completed. □

Remark 2.1. In the numerical tests below we observe optimal convergence in the L^2 norm for $\theta\neq 1/2$, where the numerical performance for $\theta=\mu$ is exactly the same as that for $\theta=1-\mu$. For the central flux, i.e. $\theta=1/2$, convergence is suboptimal for k odd, yet still optimal for k even. Hence the alternating flux $\theta=0$ or $\theta=1$ is recommended. Sub-optimal order for odd degree polynomials is also observed in [3] for the conservative DG scheme using symmetric fluxes. Note also that similar phenomena are also reported in [4,30] for the conservative DG schemes for generalized KdV equations.

Remark 2.2. In some applications, the linear equation is of the form

$$\partial_t^2 u-c^2(x)\partial_x^2 u=0,$$

which conserves the following energy functional

$$E=\frac{1}{2}\int(c^{-2}(\partial_t u)^2+(\partial_x u)^2)dx.$$

One can verify that the discrete energy, $E_h=\frac{1}{2}\int[c^{-2}(\partial_t u_h)^2+q_h^2]dx$, is conserved by the following DG scheme

$$\int c^{-2}\partial_t^2 u_h\xi dx=-\int q_h\xi_x dx-\sum_j(\hat{q}_h[\xi])_{j+1/2}, \tag{2.13a}$$

$$\int q_h\eta dx=\int\partial_x u_h\eta dx+\sum_j\left([u_h\eta]_{j+1/2}-(\hat{u_h}[\eta])_{j+1/2}\right), \tag{2.13b}$$

provided the numerical fluxes are given by

$$(\hat{q}_h,\hat{u}_h)=(q_h^\theta,u_h^{1-\theta}):=(\theta q_h^+ +(1-\theta)q_h^-,(1-\theta)u_h^+ +\theta u_h^-),\quad \theta\in[0,1], \tag{2.14}$$

with periodic boundary conditions.

2.4 Time discretization

We should choose a suitable time-stepping method such that the fully discrete scheme can preserve the energy-conserving properties of the semi-discrete system. Let $0=t_0<t_1<\cdots<t_K=T$ be a partition of the interval $[0,T]$ with time step $\Delta t=t^{n+1}-t^n$. Here uniform time step Δt is taken for convenient presentation. We define the following operator

$$D^+u_h^n=\frac{u_h^{n+1}-u_h^n}{\Delta t},\quad D^-u_h^n=\frac{u_h^n-u_h^{n-1}}{\Delta t},$$

then the fully discrete approximation u_h^n to $u(\cdot,t^n)$ is given by the second order leap-frog method: for $n=1,\cdots,K-1$, find $u_h^{n+1}\in V_h$ by

$$\int (D^+D^-u_h^n)\xi dx = -\int q_h^n (c(u_h^n)\xi)_x dx - \sum_j (\hat{q}_h^n [c(u_h^n)\xi])_{j+1/2} - \int V'(u_h^n)\xi dx, \tag{2.15a}$$

$$\int q_h^n \eta dx = \int c(u_h^n) u_{hx}^n \eta dx + \sum_j \left([C_h^n \eta]_{j+1/2} - (\hat{C}_h^n[\eta])_{j+1/2} \right), \tag{2.15b}$$

with the numerical fluxes defined in (2.10). For P^0 elements, the above LDG formulation leads to the following finite volume scheme,

$$D^+D^-u_j^n = c(u_j^n)\frac{\int_{u_j^n}^{u_{j+2}^n} c(u)du - \int_{u_{j-2}^n}^{u_j^n} c(u)du}{4h^2} - V'(u_j^n), \quad j=1,\cdots,N.$$

This when $c(u)$ is a constant c and $V(u)=\frac{\alpha}{2}u^2$ with $\alpha>0$ becomes

$$D^+D^-u_j^n = c^2\frac{u_{j+2}^n - 2u_j^n + u_{j-2}^n}{4h^2} - \alpha u_j^n.$$

By the von Neumann stability analysis, we can obtain the CFL condition

$$\Delta t \le \frac{2}{\sqrt{c^2+\alpha h^2}}h.$$

For P^k elements, the stability condition, $\Delta t \le Q(c,k)h$, can become more restrictive. In our numerical experiments, we use small time steps so that the energy preserving property can still be observed for the fully discrete scheme. Alternatively, the implicit Runge-Kutta collocation type time-stepping methods [15] or a symmetric multistep method [23] can be employed in a fully discrete scheme which does preserve the conservation properties up to round-off error.

The above method requires initial conditions for two time steps. We obtain u^1 by the Taylor expansion of u at $t=0$,

$$u(x,\Delta t) = u(x,0) + \Delta t \partial_t u(x,0) + \frac{\Delta t^2}{2}\partial_t^2 u(x,0) + \mathcal{O}(\Delta t^3), \tag{2.16}$$

and conversion of $\partial_t^2 u$ to $c(u)\partial_x(c(u)\partial_x u)$ using the wave equation, while $u(x,0)$ and $\partial_t u(x,0)$ are given by initial conditions.

More precisely, we prepare the initial data as follows:

$$u^0 = \Pi u_0, \qquad u^1 = u^0 + \Delta t \Pi u_1 + \frac{\Delta t^2}{2}\left[c(u^0)\partial_x(c(u^0)\partial_x u^0) - V'(u^0)\right], \tag{2.17}$$

where Π is the projection operator defined in (2.11). For the time step of size $\Delta t \sim h^2$, the temporal accuracy of order $(\Delta t)^2$ will not dominate over the spatial accuracy of order

h^{k+1} for $0\leq k\leq 3$. For even higher order schemes, one may use more terms in the Taylor expansion (2.16) so that the initial error is insignificant. In the Taylor expansion, the higher derivatives with respect to t can be converted to derivatives in x through repeated use of the wave equation.

2.5 Algorithm

The details related to the implementation of the method is summarized in the following algorithm.

1. First, from (2.12b), we obtain q_h in the following form

$$Q_h = A[U_h], \tag{2.18}$$

   where Q_h, U_h denote the vectors containing the degree of freedom for q_h, u_h, respectively.

2. We then substitute (2.18) into (2.12a) to obtain

$$\partial_t^2 U_h = B[A[U_h], U_h]. \tag{2.19}$$

3. A time discretization method is used to solve the obtained 2nd order semi-discrete ODE system (2.19).

3 An energy dissipating scheme

In this section, we present an energy dissipating scheme. We use a cell-wise artificial dissipation approach, motivated by some similar smoothness indicators proposed in [26, 31] in the simulation of the compressible Euler equation.

For each cell I_j, the amplitude can be modeled as

$$\epsilon_j = \begin{cases} 0 & \text{if } \Lambda_j < \Lambda_* - \kappa, \\ \frac{\epsilon_0}{2}\left(1+\sin\frac{\pi(\Lambda_j-\Lambda_*)}{2\kappa}\right) & \text{if } \Lambda_*-\kappa < \Lambda_j < \Lambda_*+\kappa, \\ \epsilon_0 & \text{if } \Lambda_j > \Lambda_*+\kappa. \end{cases}$$

Herein, Λ_j is the smoothness indicator; Λ_* is a reference value of the smoothness indicator for solutions of degree k polynomials, which is modeled as $-3\log_{10}(k)$ in this study; κ is a free parameter to control the functioning spectra of the artificial damping. Set $Q_h = u_{hx}$, on each cell we project Q_h onto P^{k-2} space to obtain $\Pi(Q_h)$, and define

$$\Lambda_j = \log_{10}\frac{\|Q_h - \Pi(Q_h)\|_{0,I_j}^2}{\|Q_h\|_{0,I_j}^2}.$$

We note that this smoothness indicator can robustly detect solution singularities, as Λ_j is much larger than Λ_* when the wave field is not smooth. The amount of artificial damping added to the equation can be modeled as

$$\epsilon_0 = h(2-h)\|c(u_h)\|_\infty/\gamma,$$

for some $\gamma > 0$.

The resulting scheme is termed as an energy dissipating scheme, which is as follows: find $u_h, q_h \in V_h$, such that $\forall \xi, \eta \in V_h$,

$$\int_{I_j} \partial_t^2 u_h \xi dx = -\int_{I_j} q_h \partial_x (c(u_h)\xi) dx + \hat{q}_h c(u_h)\xi|_{\partial I_j} - \varepsilon_j \int_{I_j} \partial_x(\partial_t u_h)\partial_x \xi dx - \int_{I_j} V'(u_h)\xi dx, \tag{3.1a}$$

$$\int_{I_j} q_h \eta dx = \int_{I_j} c(u_h)\partial_x u_h \eta dx + (\hat{C}_h - C(u_h))\eta|_{\partial I_j}, \tag{3.1b}$$

with $C'(u) = c(u)$, and the numerical flux (2.10) for both $\hat{q}_h$ and $\hat{C}_h$. The global form of the LDG formulation is

$$\begin{aligned}\int \partial_t^2 u_h \xi dx = &-\sum_{j=1}^{N} \int_{I_j} q_h \partial_x (c(u_h)\xi) dx - \sum_j (\hat{q}_h [c(u_h)\xi])_{j+1/2} \\ &- \sum_j \varepsilon_j \int_{I_j} \partial_x(\partial_t u_h)\partial_x \xi dx - \int V'(u_h)\xi dx,\end{aligned} \tag{3.2a}$$

$$\int q_h \eta dx = \sum_{j=1}^{N} \int c(u_h)\partial_x u_h \eta dx + \sum_j \left([C(u_h)\eta]_{j+1/2} - (\hat{C}_h[\eta])_{j+1/2} \right). \tag{3.2b}$$

A similar analysis to the proof of Theorem 2.1 gives

$$\frac{d}{dt}\int \left(\frac{1}{2}\left((\partial_t u_h)^2 + q_h^2 \right) + V(u_h) \right) dx = -\sum_j \varepsilon_j \int_{I_j} \partial_x (\partial_t u_h)^2 dx \le 0.$$

We again use the leap-frog method to obtain the fully discrete scheme as follows: for $n = 1, \cdots, K-1$, find $u_h^{n+1} \in V_h$ by

$$\begin{aligned}\int D^- D^+ u_h^n \xi dx = &-\int q_h^n \partial_x (c(u_h^n)\xi) dx - \sum_j (\hat{q}_h^n [c(u_h^n)\xi])_{j+1/2} \\ &- \sum_j \varepsilon_j \int_{I_j} \frac{\partial_x u_h^{n+1} - \partial_x u_h^{n-1}}{2\Delta t} \partial_x \xi dx - \int V'(u_h^n)\xi dx,\end{aligned} \tag{3.3a}$$

$$\int q_h^n \eta dx = \int c(u_h^n)\partial_x u_h^n \eta dx + \sum_j \left([C_h^n \eta]_{j+1/2} - (\hat{C}_h^n[\eta])_{j+1/2} \right), \tag{3.3b}$$

for all test functions ξ and η in V_h.

We note that our approach differs from that in [3] as they introduce a different smoothness indicator and also modify the numerical flux. The author in [20] proposed a different dissipation realized through a vanishing viscosity sequence.

4 Numerical experiments

In this section we present numerical experiments to illustrate the performance of our energy conserving and dissipating schemes. Attention is given particularly to two issues:

- Verification of the theoretical results, including a study of convergence rates and the energy conservation;
- Investigation of the long time behavior of the energy conserving scheme. This includes a comparison of the errors as a function of time, and the solution profiles after long time integration.

4.1 Convergence rates

We begin to test the order of convergence of the proposed ECLDG scheme. The results here present the case of uniform meshes, in which the domain is uniformly divided into N cells. The second order leap-frog time discretization is stable for $\Delta t \leq Q(c,k)h$; we adopt a smaller time-step by the relation $\Delta t = \mathcal{O}(h^2)$ so that the numerical error will be dominated by the spatial discretization error.

Example 4.1. We consider the linear wave equation

$$\partial_t^2 u - \partial_x^2 u = 0, \tag{4.1}$$

over the domain $(0,2\pi)\times\mathbb{R}^+$, subject to initial data

$$u(x,0) = e^{\sin x}, \quad \partial_t u(x,0) = -e^{\sin x}\cos x, \quad x\in(0,2\pi), \tag{4.2}$$

and periodic boundary conditions. The exact solution is

$$u(x,t) = e^{\sin(x-t)}.$$

With this example, we first test the effect of choices of $\theta\in[0,1]$ using P^2 polynomial approximations on uniform meshes. Table 1 reports the numerical errors and the orders of accuracy for P^2 approximation at $t=1$. Different choices of $\theta\in[0,1]$ are shown to yield the same order of accuracy, though numerical errors are slightly different. Note also that both numerical errors and orders of convergence are identical for both θ and $1-\theta$.

Next we present both the numerical errors and the orders of convergence in Table 2, using $P^k(0\leq k\leq 3)$ polynomials and the numerical flux (2.10) with different $\theta=0,1/4,1/2$. We see that there is an order loss for polynomials of odd degree with $\theta=1/2$.

We also verify the conservative property of the LDG method. Figs. 1 and 3 plot the numerical solutions at $t=0,100,1000$ and $t=5000$ with $k=2$ and $k=3$, respectively. It shows that the scheme gives quite a good approximation to the exact solution in the long time simulation. We plot in Figs. 2 and 4 the energy and L^2 error from $t=0$ to $t=5000$. It shows that the discrete energy is conserved by the ECLDG method, and the L^2 error increases linearly with time.

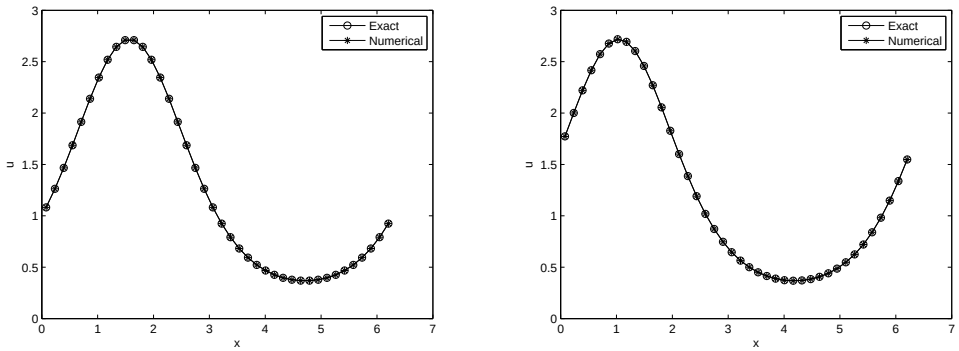

(a) $t=0$ (b) $t=100$

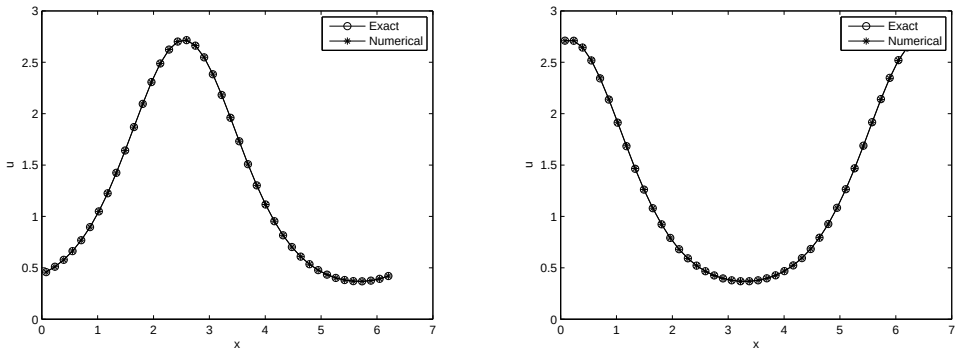

(c) $t=1000$ (d) $t=5000$

Figure 1: Example 4.1, the solutions at $t=0,100,1000$ and 5000 with $k=2$, $\Delta t=2.5\times10^{-3}$ and 40 cells.

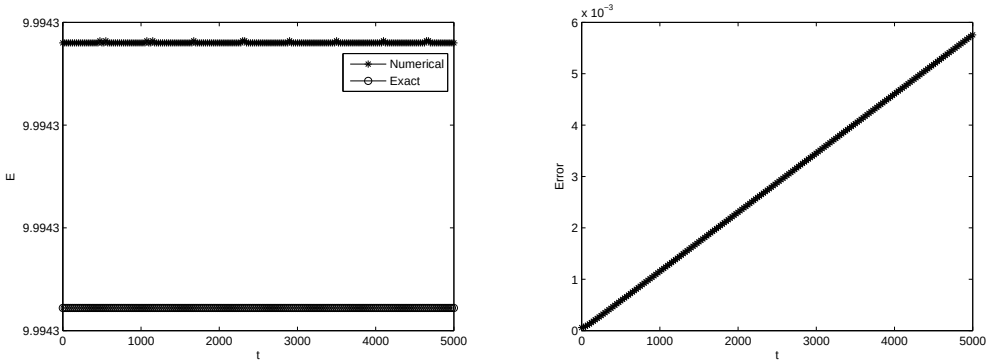

(a) Energy history (b) L^2 errors

Figure 2: Example 4.1, time history of the L^2 error and energy plots using the conservative LDG (2.15) with $k=2$, $\Delta t=2.5\times10^{-3}$ and 40 cells.

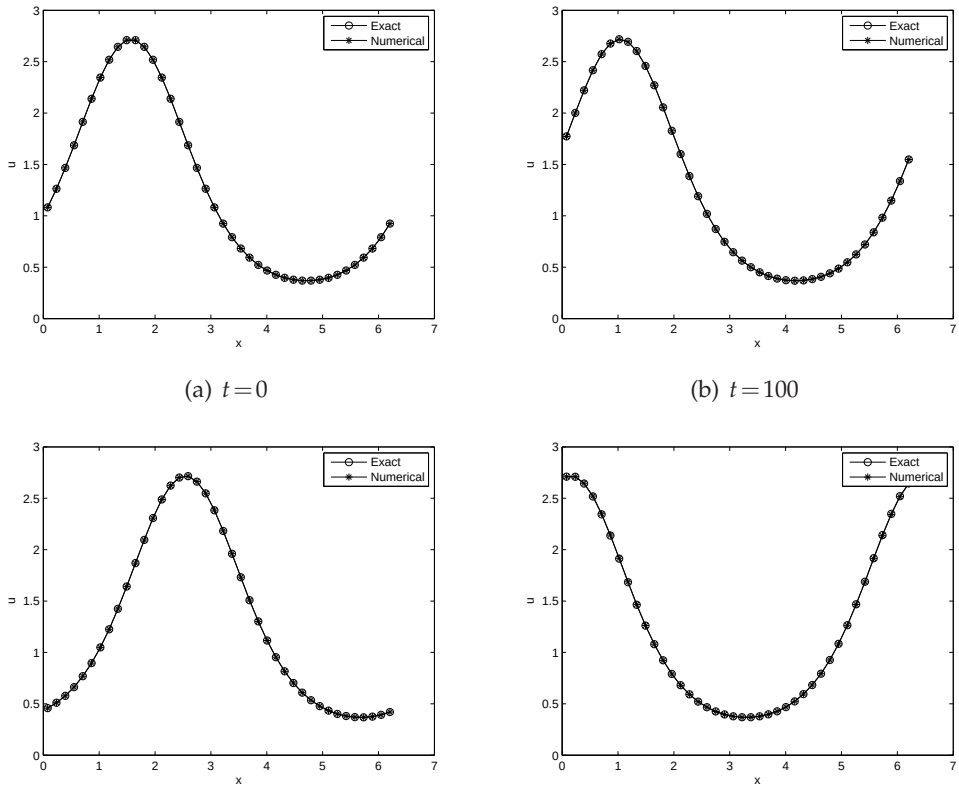

(a) $t=0$ (b) $t=100$

(c) $t=1000$ (d) $t=5000$

Figure 3: Example 4.1, the solutions at $t=0,100,1000$ and 5000 with $k=3$, $\Delta t=2.5\times10^{-3}$ and 40 cells.

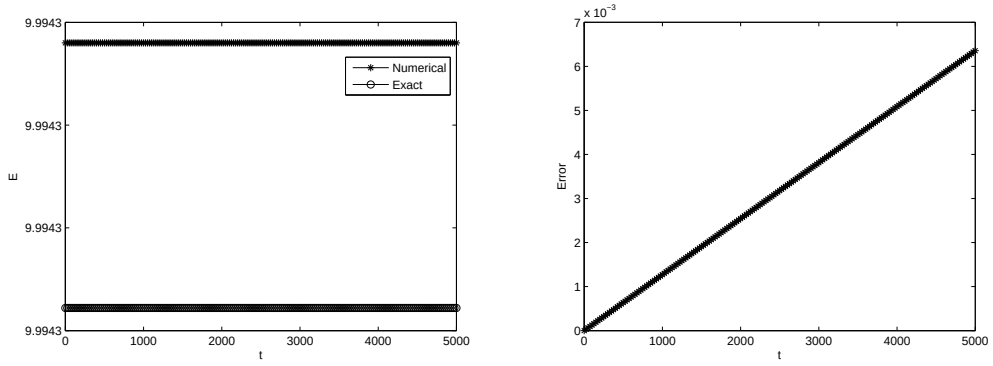

(a) Energy history (b) L^2 errors

Figure 4: Example 4.1, time history of the L^2 error and energy plots using the conservative LDG (2.15) with $k=3$, $\Delta t=2.5\times10^{-3}$ and 40 cells.

Table 1: Errors for Example 4.1 when using P^2 polynomials on a uniform mesh of N cells. Final time is $t=1$.

θ	N	L^2 error	order	θ	N	L^2 error	order
$\theta=0$	10	7.45e-03	-	$\theta=1$	10	7.45e-03	-
	20	7.71e-04	3.27		20	7.71e-04	3.27
	40	9.31e-05	3.05		40	9.31e-05	3.05
	80	1.29e-05	2.85		80	1.29e-05	2.85
	160	1.63e-06	2.98		160	1.63e-06	2.98
	320	2.33e-07	2.81		320	2.33e-07	2.81
$\theta=\frac{1}{5}$	10	6.57e-03	-	$\theta=\frac{4}{5}$	10	6.57e-03	-
	20	7.55e-04	3.12		20	7.55e-04	3.12
	40	8.52e-05	3.15		40	8.52e-05	3.15
	80	9.36e-06	3.19		80	9.36e-06	3.19
	160	1.31e-06	2.84		160	1.31e-06	2.84
	320	1.67e-07	2.97		320	1.67e-07	2.97
$\theta=\frac{2}{5}$	10	7.97e-03	-	$\theta=\frac{3}{5}$	10	7.97e-03	-
	20	5.42e-04	3.88		20	5.42e-04	3.88
	40	6.38e-05	3.09		40	6.38e-05	3.09
	80	7.88e-06	3.02		80	7.88e-06	3.02
	160	1.00e-06	2.98		160	1.00e-06	2.98
	320	1.23e-07	3.02		320	1.23e-07	3.02
$\theta=\frac{1}{4}$	10	7.03e-03	-	$\theta=\frac{3}{4}$	10	7.03e-03	-
	20	6.50e-04	3.44		20	6.50e-04	3.44
	40	7.17e-05	3.18		40	7.17e-05	3.18
	80	1.01e-05	2.83		80	1.01e-05	2.83
	160	1.24e-06	3.03		160	1.24e-06	3.03
	320	1.44e-07	3.11		320	1.44e-07	3.11
$\theta=\frac{1}{3}$	10	7.43e-03	-	$\theta=\frac{2}{3}$	10	7.43e-03	-
	20	5.66e-04	3.71		20	5.66e-04	3.71
	40	6.81e-05	3.06		40	6.81e-05	3.06
	80	8.18e-06	3.06		80	8.18e-06	3.06
	160	1.00e-06	3.03		160	1.00e-06	3.03
	320	1.28e-07	2.97		320	1.28e-07	2.97

4.2 Time history of the energy

We next investigate the long time evolution of the rescaled energy $E=\int(\partial_t u_h)^2+q_h^2 dx$ of both the conservative and dissipative schemes.

Example 4.2. Consider the nonlinear wave equation (1.1), i.e.,

$$\partial_t^2 u - c(u)\partial_x(c(u)\partial_x u)=0,$$

with smooth initial data

$$u(x,0)=\frac{\pi}{4}+\exp(-x^2), \tag{4.3}$$

Table 2: Errors for Example 4.1 when using P^k polynomials on a uniform mesh of N cells. Final time is $t=1$.

(k,θ)		Δt	4.0e-2	1.0e-2	2.5e-3	6.25e-4	1.5625e-4	3.90625e-05
		N	10	20	40	80	160	320
$k=0$	$\theta=0$	$\|u-u_h\|$	4.09e-1	2.03e-1	1.01e-1	5.07e-2	2.53e-2	1.27e-2
		order	-	1.01	1.01	0.99	1.00	0.99
	$\theta=\frac{1}{4}$	$\|u-u_h\|$	4.67e-1	2.15e-1	1.03e-1	5.09e-2	2.54e-2	1.27e-2
		order	-	1.12	1.06	1.02	1.00	1.00
	$\theta=\frac{1}{2}$	$\|u-u_h\|$	5.00e-1	2.21e-1	1.04e-1	5.10e-2	2.54e-2	1.27e-2
		order	-	1.18	1.09	1.03	1.01	1.00
$k=1$	$\theta=0$	$\|u-u_h\|$	8.80e-2	2.19e-2	5.35e-3	1.20e-3	2.82e-4	7.68e-5
		order	-	2.01	2.03	2.16	2.09	1.88
	$\theta=\frac{1}{4}$	$\|u-u_h\|$	1.10e-1	3.76e-2	7.95e-3	2.10e-3	4.73e-4	1.22e-4
		order	-	1.55	2.24	1.92	2.15	1.95
	$\theta=\frac{1}{2}$	$\|u-u_h\|$	1.67e-1	8.60e-2	4.33e-2	2.17e-2	1.08e-2	5.42e-03
		order	-	0.96	0.99	1.00	1.01	1.00
$k=2$	$\theta=0$	$\|u-u_h\|$	7.45e-3	7.71e-4	9.31e-5	1.29e-5	1.63e-6	2.33e-07
		order	-	3.27	3.05	2.85	2.98	2.81
	$\theta=\frac{1}{4}$	$\|u-u_h\|$	7.03e-3	6.50e-4	7.17e-5	1.01e-5	1.24e-6	1.44e-07
		order	-	3.44	3.18	2.83	3.03	3.11
	$\theta=\frac{1}{2}$	$\|u-u_h\|$	8.78e-3	5.54e-4	6.11e-5	7.50e-6	9.35e-7	1.16e-07
		order	-	3.99	3.18	3.03	3.00	3.01
$k=3$	$\theta=0$	$\|u-u_h\|$	8.15e-4	4.59e-5	3.01e-6	1.87e-7	1.28e-8	7.07e-10
		order	-	4.15	3.93	4.01	3.87	4.18
	$\theta=\frac{1}{4}$	$\|u-u_h\|$	8.29e-4	5.81e-5	4.42e-6	2.98e-7	2.12e-8	1.37e-9
		order	-	3.83	3.72	3.89	3.81	3.95
	$\theta=\frac{1}{2}$	$\|u-u_h\|$	8.18e-4	8.78e-5	9.50e-6	8.74e-7	1.01e-7	1.23e-8
		order	-	3.22	3.21	3.40	3.11	3.04

$$\partial_t u(x,0) = -c(u(x,0))\partial_x u(x,0), \quad x\in\mathbb{R}, \tag{4.4}$$

where

$$c^2(u) = \alpha\cos^2 u + \beta\sin^2 u.$$

This problem has been tested numerically in [3,17,22]. The exact solution is not available, we use a reference solution computed on a finer mesh with $N=20000$. Table 3 shows errors and the rate of convergence for the ECLDG scheme using central numerical fluxes, i.e., (2.10) with $\theta=1/2$. For $k=1$, it exhibits sub-optimal convergence rate. For $k=0,2$, the order of convergence is optimal $k+1$.

Figs. 5-6 show the discrete energy and numerical solutions when using the conservative LDG schemes, and Figs. 9-10 when using the dissipative LDG schemes. Also Figs. 7-8 show the numerical solutions of the auxiliary variable $q=c(u)u_x$ at times $t=0$, $t=5$, $t=6$ and $t=15$ for the conservative and dissipative LDG schemes, respectively. The results

Table 3: Errors $\|u-u_{ref}\|$ for Example 4.2 with $(\alpha,\beta)=(0.5,1.5)$ when using P^k polynomials on a uniform mesh of N cells. Final time is $t=1$. The reference solution was computed with $N=20000$.

$k=0$	N	125	250	500	1000
	$\|u-u_h\|$	2.87e-2	1.07e-2	4.78e-3	2.30e-3
	order	-	1.42	1.16	1.06
$k=1$	N	125	250	500	1000
	$\|u-u_h\|$	6.93e-3	3.21e-3	1.57e-3	7.82e-4
	order	-	1.11	1.03	1.01
$k=2$	N	125	250	500	1000
	$\|u-u_h\|$	1.09e-3	1.17e-4	1.40e-5	1.36e-6
	order	-	3.22	3.06	3.35

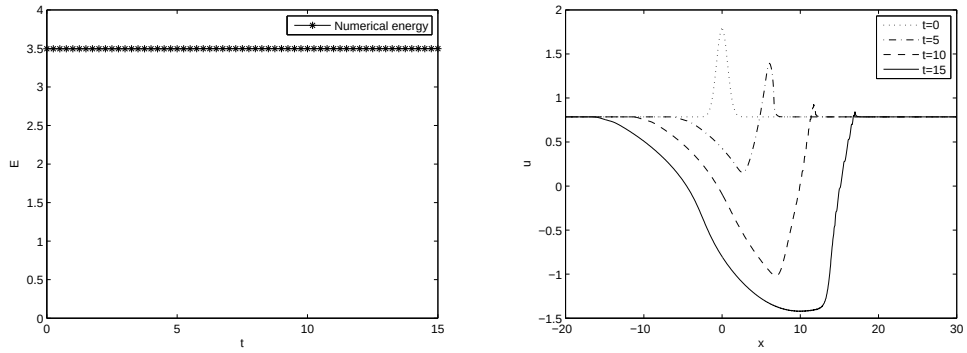

(a) Energy history (b) Solution

Figure 5: Example 4.2, $(\alpha,\beta)=(0.5,1.5)$, time history of energy and numerical solutions plots using the conservative LDG (2.15) with $k=2$, $\Delta t=1.0\times10^{-3}$ and 1000 cells.

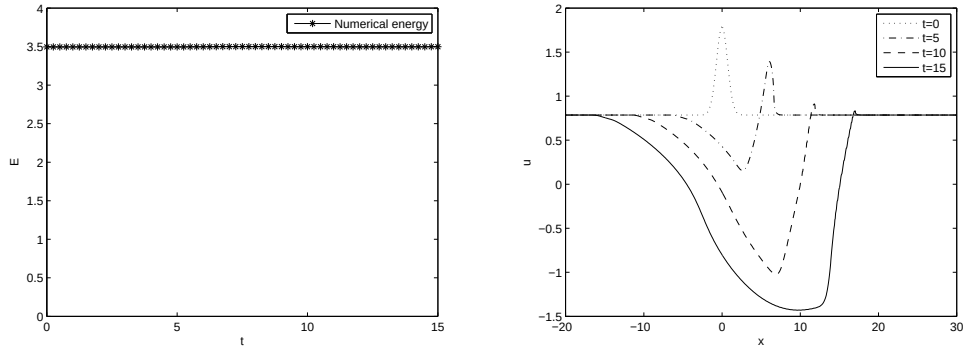

(a) Energy history (b) Solution

Figure 6: Example 4.2, $(\alpha,\beta)=(0.5,1.5)$, time history of energy and numerical solutions plots using the conservative LDG (2.15) with $k=3$, $\Delta t=1.0\times10^{-3}$ and 1000 cells.

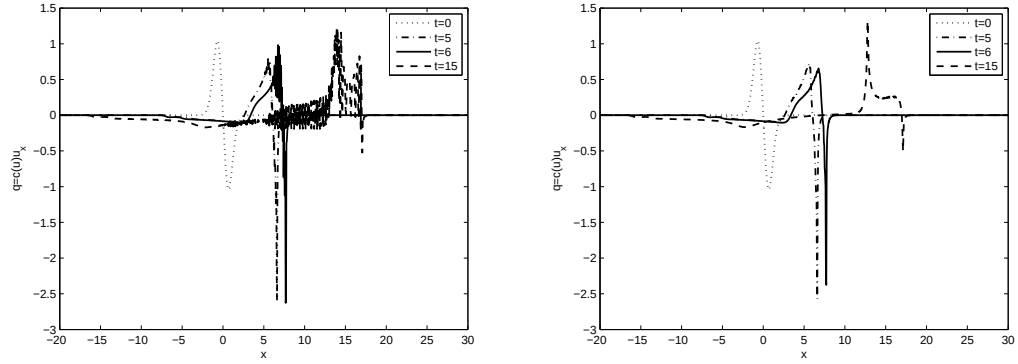

(a) Conservative LDG scheme (b) Dissipative LDG scheme

Figure 7: Example 4.2, $(\alpha,\beta)=(0.5,1.5)$, numerical solutions q_h plots using the conservative LDG scheme (2.15) and the dissipative LDG scheme (3.3) with $k=2$, $\Delta t=2.5\times10^{-3}$ and 1000 cells.

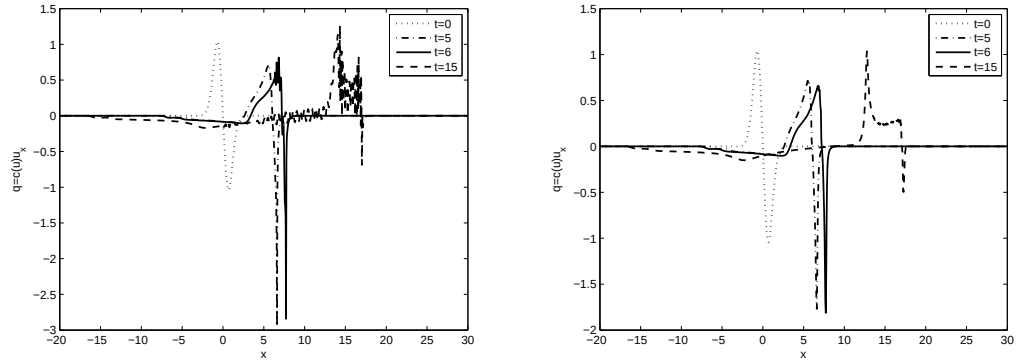

(a) Conservative LDG scheme (b) Dissipative LDG scheme

Figure 8: Example 4.2, $(\alpha,\beta)=(0.5,1.5)$, numerical solutions q_h plots using the conservative LDG scheme (2.15) and the dissipative LDG scheme (3.3) with $k=3$, $\Delta t=2.5\times10^{-3}$ and 1000 cells.

are consistent with those reported in [3, 22]. It is reported that despite the initial data is smooth, the solution develops a singularity in u_x around $t=6$. After this time, we see that numerical solution of q_h displays numerical oscillations when conservative schemes are used. These oscillations are not present when using the dissipative scheme. For the time evolution of the discrete energy, the conservative scheme shows its conservation, but the dissipative scheme shows that it decreases in time.

It is known that the nonlinear variational wave equation admits both conservative and dissipative weak solutions, we refer to [3, 20] for related numerical results on these two solutions. Fig. 11 shows the numerical solution to 4.2 with $(\alpha=0.5, \beta=4.5)$ using the conservative LDG (2.15) and the dissipative LDG (3.3). The results show that the so-

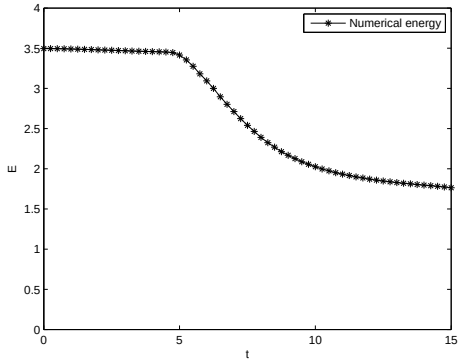

(a) Energy history

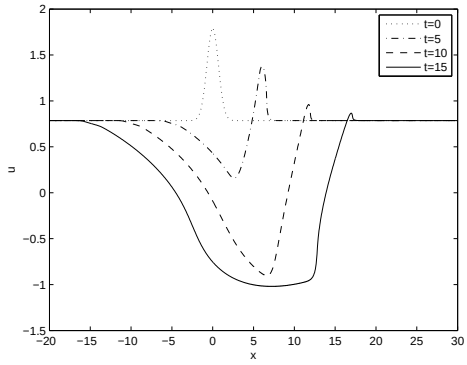

(b) Solution

Figure 9: Example 4.2, $(\alpha,\beta)=(0.5,1.5)$, time history of energy and numerical solutions plots using the dissipative LDG scheme (3.3) with $k=2$, $\Delta t=2.5\times10^{-3}$ and 1000 cells.

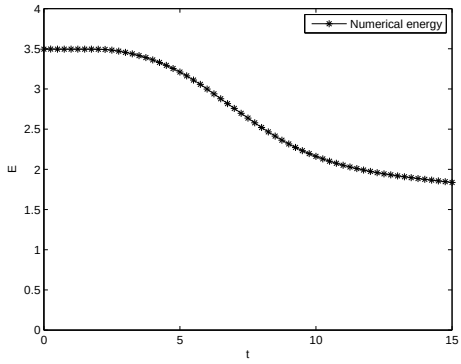

(a) Energy history

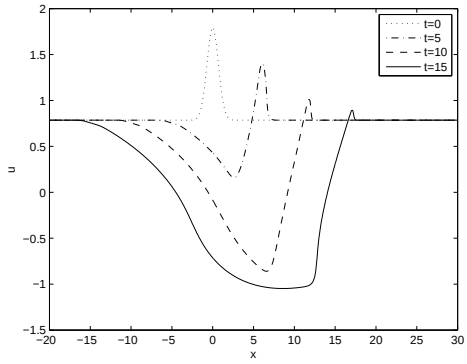

(b) Solution

Figure 10: Example 4.2, $(\alpha,\beta)=(0.5,1.5)$, time history of energy and numerical solutions plots using the dissipative LDG scheme (3.3) with $k=3$, $\Delta t=2.5\times10^{-3}$ and 1000 cells.

lution may develop a singularity at a time $4<t<6$, see Fig. 11(a, b). After the formation of singularity we see that the conservative and dissipative LDG schemes give two distinct solutions, as shown in Fig. 11(c, d). From Fig. 12, we see that solutions obtained with various values of time steps Δt are almost indistinguishable. We also observe a large deviation between conservative and dissipative solutions. These show that the two schemes converge to different solutions as $\Delta t\to0$.

Example 4.3. We consider a problem numerically investigated previously in [3, 18]. We look for traveling wave solutions of the form $u(x,t)=U(x-st)$ to (1.1), with $c(u)$ given by

$$c^2(u)=\alpha\cos^2u+\beta\sin^2u,$$

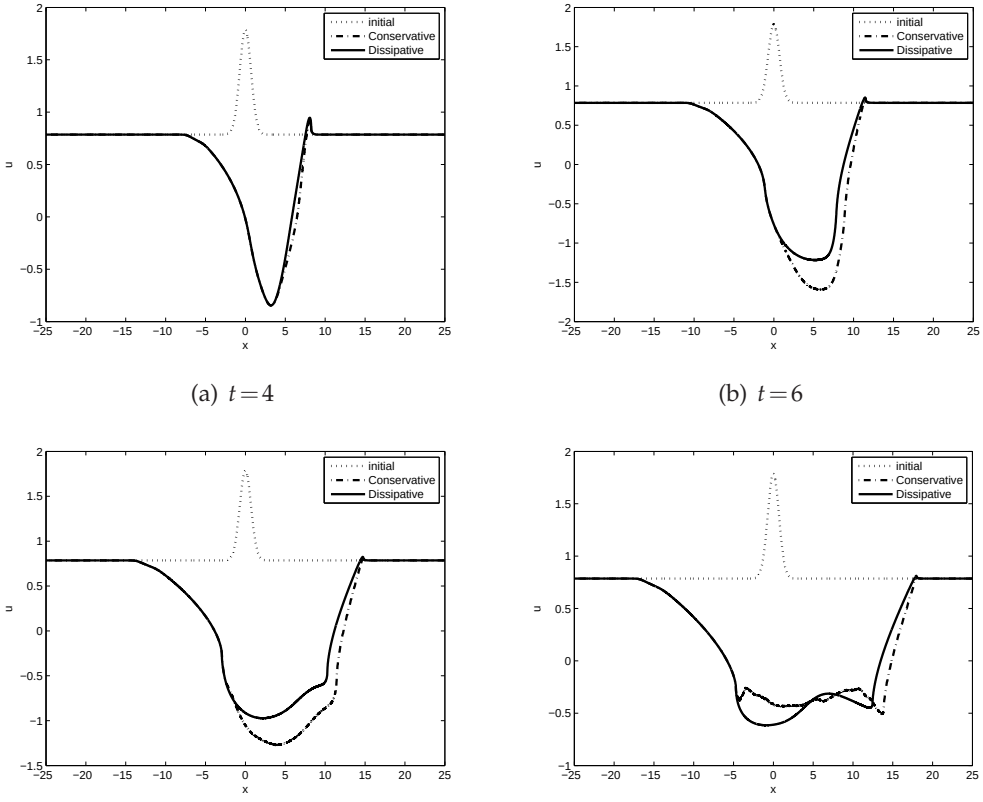

(a) $t=4$ (b) $t=6$

(c) $t=8$ (d) $t=10$

Figure 11: Example 4.2, $(\alpha,\beta)=(0.5,4.5)$, numerical solution plots using the conservative LDG scheme (2.15) and the dissipative LDG scheme (3.3) with $k=2$, $\Delta t=1.0\times10^{-3}$ and 5000 cells.

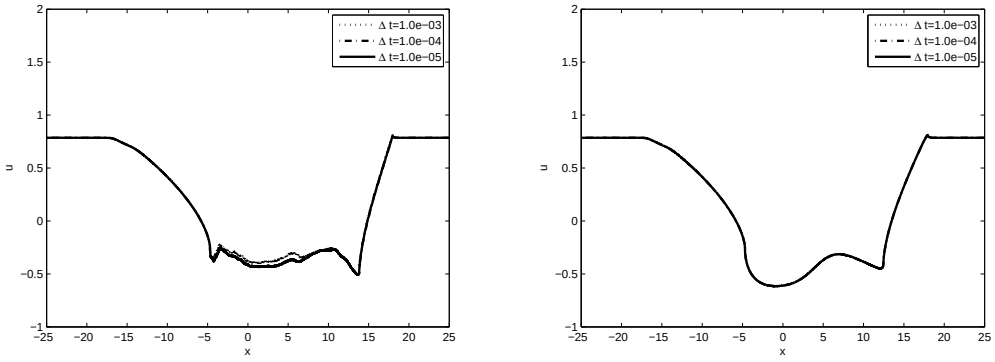

(a) Conservative LDG scheme (b) Dissipative LDG scheme

Figure 12: Example 4.2, $(\alpha,\beta)=(0.5,4.5)$, numerical solutions u_h at $t=10$ plots using the conservative LDG scheme (2.15) and the dissipative LDG scheme (3.3) with $k=2$ and 5000 cells.

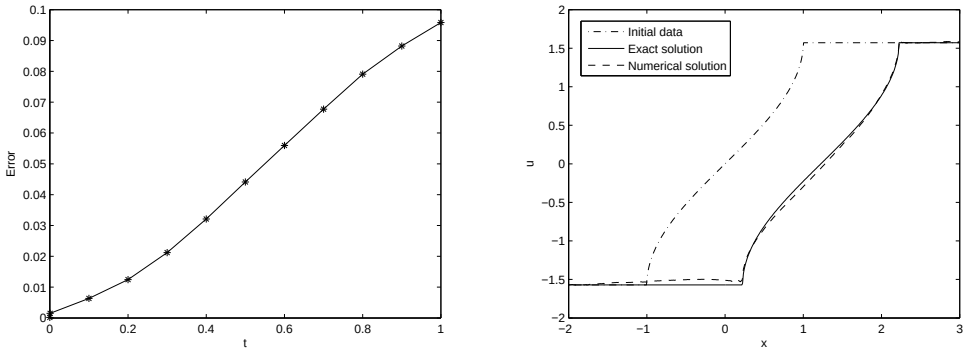

(a) L^2 errors (b) Solution

Figure 13: Example 4.3, time history of the L^2 error and numerical solutions plots at $t=1$ using the conservative LDG (2.15) with $k=3$, $\Delta t=1.0\times10^{-3}$ and 500 cells.

then U must satisfy

$$U'\sqrt{|s^2-\alpha\cos^2U-\beta\sin^2U|}=A,$$

where A is some integration constant.

For $s=\sqrt{\alpha}$, we have

$$U'\sin(U)=\frac{A}{\sqrt{|\alpha-\beta|}}.$$

Integration of this with boundary conditions $U(0)=0$ and $U(1)=\pi$ gives an explicit traveling wave solution

$$U(\xi)=\cos^{-1}(-2\xi+1),\quad 0<\xi=x-st<1,$$

connecting 0 for $\xi\leq0$ and π for $\xi\geq1$.

For $s=\sqrt{\beta}$, we have

$$U'\cos(U)=\frac{A}{\sqrt{|\alpha-\beta|}}.$$

Integration of this with boundary conditions $U(-1)=-\pi/2$ and $U(1)=\pi/2$ gives an explicit traveling wave solution

$$U(\xi)=\sin^{-1}(\xi),\quad 0<\xi=x-st<1,$$

connecting $-\pi/2$ for $\xi\leq0$ and $\pi/2$ for $\xi\geq1$.

Fig. 13 shows the L^2 error history and numerical solution at $t=1$ with $N=500$ using the conservative LDG scheme with P^3 approximation. The numerical solutions are comparable with those reported in [3].

Finally, we present an example for the case with constant speed c, but with non-trivial $V(u)$.

Example 4.4. We consider the Sine-Gordon equation

$$\partial_t^2 u - c^2 \partial_x^2 u + \sin u = 0. \tag{4.5}$$

This equation appears in several physical applications (see e.g. [16]), and one interesting feature of the sine-Gordon equation is the existence of soliton and multi-soliton solutions. The equation can be solved exactly by various analytical techniques, since the direct method introduced in [21].

We apply the explicit scheme (2.15) to solve (4.5) with appropriate boundary conditions. Let us solve it on the interval $[-L,L]$ with Dirichlet boundary conditions using the following parameters set:

$$L=20, \quad c=0.2, \quad \Delta x=0.1, \quad \Delta t=0.01.$$

We start with the numerical representation of kink and antikink solutions. A one-soliton solution of the Sine-Gordon equation,

$$u(x,t)=4\arctan\left(e^{\frac{x-ct}{\sqrt{1-c^2}}}\right),$$

for which u increases monotonically from zero to 2π as x increases from $-\infty$ to ∞, is called a kink. A solution of the form

$$u(x,t)=4\arctan\left(e^{-\frac{x-ct}{\sqrt{1-c^2}}}\right)$$

called an antikink, in contrast to the kink, is the transition from the solution 2π to 0.

Table 4 reports the numerical errors and the orders of accuracy for P^k approximation to kink solutions. We clearly see that the convergence rate is $k+1$ for even values of $k=0,2$, but only k for odd value of $k=1$, while central numerical fluxes are used.

Fig. 14 shows the space-time plot of the numerical kink and antikink solutions, respectively. Direct comparisons between the numerical solutions and the analytical solutions show good agreement.

We next produce two-solitons solutions, corresponding to kink-kink and kink-antikink collisions. For the kink-kink collision we choose

$$\begin{aligned}
u(x,0)&=4\arctan\left(e^{\frac{x+L/2}{\sqrt{1-c^2}}}\right)+4\arctan\left(e^{\frac{x-L/2}{\sqrt{1-c^2}}}\right),\\
\partial_t u(x,0)&=-2\frac{c}{\sqrt{1-c^2}}sech\left(\frac{x+L/2}{\sqrt{1-c^2}}\right)+2\frac{c}{\sqrt{1-c^2}}sech\left(\frac{x-L/2}{\sqrt{1-c^2}}\right),
\end{aligned}$$

and for the kink-antikink collision the initial conditions are

$$\begin{aligned}
u(x,0)&=4\arctan\left(e^{\frac{x+L/2}{\sqrt{1-c^2}}}\right)+4\arctan\left(e^{-\frac{x-L/2}{\sqrt{1-c^2}}}\right),\\
\partial_t u(x,0)&=-2\frac{c}{\sqrt{1-c^2}}sech\left(\frac{x+L/2}{\sqrt{1-c^2}}\right)-2\frac{c}{\sqrt{1-c^2}}sech\left(\frac{x-L/2}{\sqrt{1-c^2}}\right).
\end{aligned}$$

Table 4: Errors for Example 4.4 with kink solutions when using P^k polynomials on a uniform mesh of N cells. Final time is $t=1$.

$k=0$	Δt	1.0e-1	5.0e-2	2.5e-2	1.25e-2	6.25e-3
	N	100	200	400	800	1600
	$\|u-u_h\|$	3.37e-1	1.66e-1	8.26e-2	4.13e-2	2.06e-2
	order	-	1.02	1.01	1.00	1.00
$k=1$	Δt	1.0e-1	5.0e-2	2.5e-2	1.25e-2	6.25e-3
	N	100	200	400	800	1600
	$\|u-u_h\|$	7.13e-2	3.63e-2	1.83e-2	9.18e-3	4.60e-3
	order	-	0.97	0.99	1.00	1.18
$k=2$	Δt	1.0e-1	2.5e-2	6.25e-3	1.5625e-3	3.90625e-4
	N	100	200	400	800	1600
	$\|u-u_h\|$	4.28e-3	5.34e-5	6.43e-6	8.01e-7	1.00e-7
	order	-	6.32	3.05	3.00	3.00

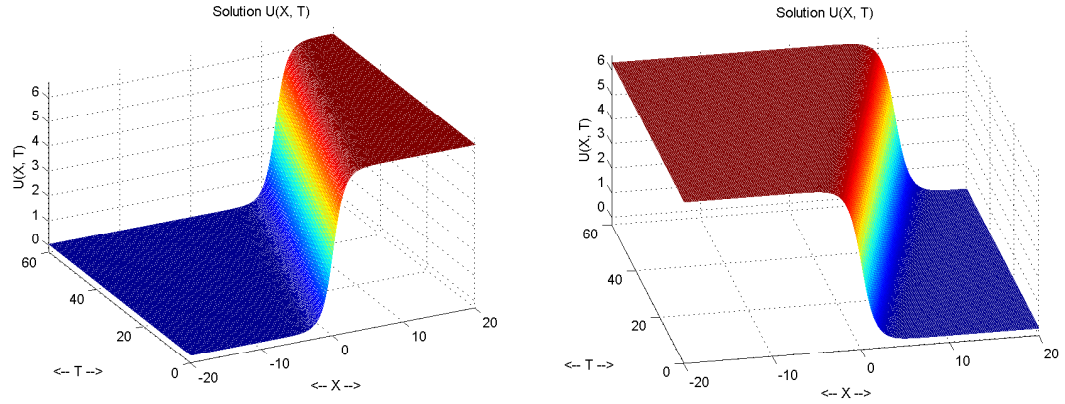

(a) Kink soliton (b) Antikink soliton

Figure 14: Example 4.4, single soliton, numerical solutions calculated with $k=2$, $\Delta t=1.0\times10^{-2}$ and 400 cells.

Numerical solutions corresponding to both cases are presented in Fig. 15, respectively. It can be seen that no spurious oscillations are observed. In the kink-kink simulation, the kinks move toward each other with equal velocities. Eventually they collide, whereby they are reflected and move away form one another. In the kink-antikink simulation, the kink and the antikink initially move inward towards the origin. As they collide, the profile instantaneously becomes equal to 2π. Subsequently the kink and the antikink move away form one another in their original directions of motion. Fig. 15 is in agreement with [2].

The sine-Gordon equation also has another group of soliton solutions, known as breathers. A breather is a nonlinear mode that is localized in space and oscillates with

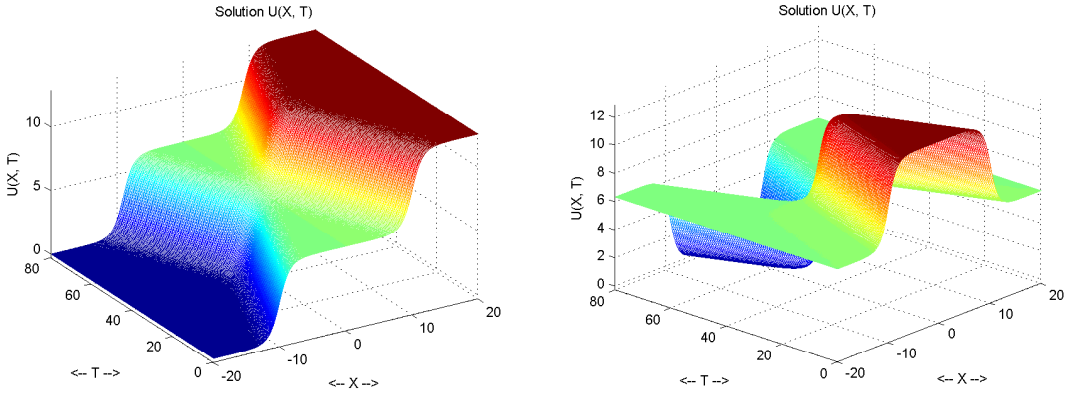

(a) Kink-kink collision (b) Kink-antikink collision

Figure 15: Example 4.4, soliton collision, numerical solutions calculated with $k=2$, $\Delta t=1.0\times10^{-2}$ and 400 cells.

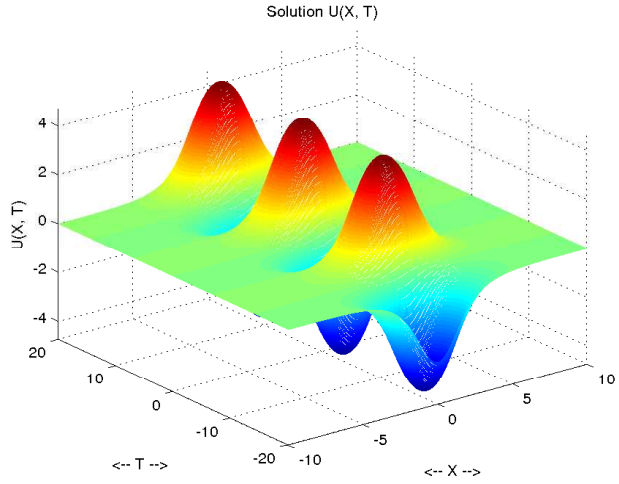

Breather soliton

Figure 16: Example 4.4, breather soliton, numerical solutions calculated with $k=2$, $\Delta t=5.0\times10^{-3}$ and 200 cells.

time. We consider equation (4.5) in the domain $-10\leq x\leq 10, -20\leq t\leq 20$. The exact solution is

$$u(x,t)=4\arctan\left(\frac{1}{c}\sin\left(\frac{ct}{\sqrt{1+c^2}}\right)sech\left(\frac{x}{\sqrt{1+c^2}}\right)\right),\quad c=0.5.$$

The initial and boundary conditions are derived from the exact solution. Fig. 16 shows the space-time profile of the numerical solution for $x\in[-10,10]$ and $t\in[-20,20]$. We

can see that no spurious oscillations and shift of the solitons is observed, which is in agreement with the corresponding result in [2].

5 Concluding remarks

In this paper, we have developed an energy conserving LDG method for solving the nonlinear variational wave equation. The scheme is constructed for a generalized wave equation, also including linear wave equation with variable wave speed, and the sine-Gordon equation. The energy conserving property for the semi-discrete formulation can be proven. The leap-frog time discretization was used to obtain a fully discrete method. A dissipative scheme is also introduced by locally imposing some numerical "damping" in the conservative scheme, in order to suppress the numerical oscillations near the solution singularity. Numerical tests have demonstrated the optimal convergence for a class of alternating numerical fluxes, and the suboptimal convergence for polynomials of odd degree when the central flux is adopted. Numerical simulations with long time integration indicate that energy conserving property is important in order to accurately capture the underlying wave shapes.

Acknowledgments

Yi's research was partially supported by NSFC Project (11671341, 91430213), Hunan Provincial NSF Project (2015JJ2145) and Hunan Education Department Project (16A206). Liu's research was partially supported by the National Science Foundation under grant DMS-1312636 and the NSF Research Network Grant no. RNMS11-07291(KI-Net).

References

[1] D. Appelö and T. Hagstrom. A new discontinuous Galerkin formulation for wave equations in second order form. *SIAM J. Numer. Anal.*, 53:2705–2726, 2015.
[2] J. Argyris and M. Haase. An engineer's guide to soliton phenomena: application of the finite element method. *Comput Methods Appl. Mech. Eng.* 61:71–122, 1987.
[3] P. Aursand and U. Koley. Local discontinuous Galerkin schemes for a nonlinear variational wave equation modeling liquid crystals. *arXiv:1402.7243*, 2015.
[4] J. Bona, H. Chen, O. Karakashian, and Y. Xing. Conservative, discontinuous-Galerkin methods for the generalized Korteweg-de Vries equation. Math. Comp., 82(283):1401–1432, 2013.
[5] A. Bressan, G. Chen, and Q. Zhang. Unique conservative solutions to a variational wave equation. *Arch. Rational Mech. Anal.*, 217(3): 1069–1101, 2015.
[6] A. Bressan and Y. Zheng. Conservative solutions to a nonlinear variational wave equation. *Commun. Math. Phys.* 266:471–497, 2006.
[7] A. Bressan and T. Huang. Representation of dissipative solutions to a nonlinear variational wave equation. *arXiv:1407.1220* , 2014.
[8] Eric T. Chung and B. Engquist. Optimal discontinuous Galerkin methods for wave propagation. *SIAM Journal on Numerical Analysis*, 44:2131–2158, 2006.

[9] Eric T. Chung and B. Engquist. Optimal discontinuous Galerkin methods for the acoustic wave equation in higher dimensions. *SIAM Journal on Numerical Analysis*, 47:3820–3848, 2009.
[10] C.S. Chou, C.W. Shu and Y.L. Xing. Optimal energy conserving local discontinuous Galerkin methods for second-order wave equation in heterogeneous media. *J. Comput. Phys.* 272:88–107, 2014.
[11] B. Cockburn and C.W. Shu. TVB Runge-Kutta local projection discontinuous Galerkin finite element method for conservation laws II: general framework. *Math. Comp.*, 52:411–435, 1989.
[12] B. Cockburn and S.Y. Lin and C.W. Shu. TVB Runge–Kutta local projection discontinuous Galerkin finite element method for conservation laws III: one dimensional systems. *J. Comput. Phys.*, 84:90–113, 1989.
[13] B. Cockburn and S. Hou and C.W. Shu. The Runge–Kutta local projection discontinuous Galerkin finite element method for conservation laws IV: the multidimensional case. *Math. Comput.*, 54:545–581, 1990.
[14] B. Cockburn and C.W. Shu. The Runge–Kutta discontinuous Galerkin method for conservation laws V: multidimensional systems. *J. Comput. Phys.*, 141:199–224, 1998.
[15] K. Dekker and J.G. Verwer. Stability of Runge-Kutta methods for stiff nonlinear differential equations. North Holland, 1984.
[16] R. K. Dodd, J. C. Eilbeck, J. D. Gibbon, and H. C. Morris. Solitons in Nonlinear Wave Equations. Academic Press, New York, 1982.
[17] R. T. Glassey, J. K. Hunter and Y. Zheng. Singularities in a nonlinear variational wave equation. *J. Differential Equations*, 129, 49–78, 1996.
[18] R. Glassey, J. Hunter, and Y. Zheng. Singularities and Oscillations in a nonlinear variational wave equation. In the series The IMA Volumes in Mathematics and its Applications on Singularities and Oscillations, 91:37–60, 1997.
[19] M. J. Grote, A. Schneebeli and D. Schötzau. Discontinuous Galerkin finite element method for the wave equation. *SIAM J. Numer. Anal.* 44(6):2408–2431, 2006.
[20] T. Hagstrom. Numerical experiments on a nonlinear wave equation. *Preprint.*, 2016.
[21] R. Hirota. Exact solution of the Sine-Gordon equation for multiple collisions of solitons. *J. Phys. Soc. Jpn*, 33: 1459–1463, 1972.
[22] H. Holden, K.H. Karlsen and N.H. Risebro. A convergent finite-difference method for a nonlinear variational wave equation. *IMA J. Numer. Anal.* 29:539–572, 2009.
[23] E. Hairer, C. Lubich and G. Wanner. Geometric Numerical Integration. Springer-Verlag, Berlin, 2002.
[24] H. Holden and X. Raynaud. Global semigroup of conservative solutions of the nonlinear variational wave equation. *Arch. Rational Mech. Anal.*, 201: 871–964, 2011.
[25] U. Koley, S. Mishra, N.H. Risebro and F. Weber. Robust finite-difference schemes for a nonlinear variational wave equation modeling liquid crystals. *arXiv:1311.1766* , 2013.
[26] P.-O. Persson and J. Peraire. Sub-Cell shock capturing for discontinuous Galerkin methods. in 44th AIAA Aerospace Sciences Meeting and Exhibit, Reno, Nevada, 2006, AIAA-2006-0112.
[27] B. Riviere and M.F. Wheeler. Discontinuous finite element methods for acoustic and elastic wave problems. *Contemporary Mathematics* 329:271–282, 2003.
[28] R. A. Saxton. Dynamic instability of the liquid crystal director. Contemporary Mathematics Vol 100, Current Progress in Hyperbolic Systems, pp. 325-330, ed. W. B. Lindquist, AMS, Providence, 1989.
[29] Y.L. Xing, C.S. Chou and C.W. Shu. Energy conserving local discontinuous Galerkin meth-

ods for wave propagation problems. *Inverse Probl. Imaging* 7:967–986, 2013.
[30] N. Yi, Y. Huang and H. Liu. A direct discontinuous Galerkin method for the generalized Korteweg-de Vries equation: Energy conservation and boundary effect. *J. Comput. Phys.* 242:351–366, 2013.
[31] M. Yu and Z.J. Wang. Shock capturing for the correction procedure via reconstruction method using artificial viscosity and diffusivity. in Proceedings of the 8th International Conference on CFD, ICCFD8-2014-007
[32] G. B. Whitham. Linear and Nonlinear Waves. Wiley-Interscience, New York, 1999.
[33] P. Zhang and Y. Zheng. Weak solutions to a nonlinear variational wave equation. *Arch. Rat. Mech. Anal.* 166:303–319, 2003.
[34] P. Zhang and Y. Zheng. Weak solutions to a nonlinear variational wave equation with general data. *Ann. Inst. H. Poincare Anal. Non Lineaire* 22:207–226, 2005.